Colloidal model for nucleation and aggregation in one dimension: Accessing the interaction parameters

Juan David Álvarez-Cuartas [1,*] Manuel Camargo [2,†] and Diego Luis González-Cabrera [1,‡]
[1]*Departamento de Física, Universidad del Valle, Apartado Aéreo 25360, Cali, Colombia*
[2]*DCA and CICBA, Universidad Antonio Nariño–Campus Farallones, Km 18 Vía Cali-Jamundí, Cali 760030, Colombia*

(Received 13 February 2024; accepted 2 May 2024; published 6 June 2024)

Through a one-dimensional colloidal model for epitaxial growth, we characterize the nucleation and aggregation processes occurring in a gap between adjacent islands. The timescales associated with deposition, diffusion, aggregation, and nucleation inside the gap are studied in terms of the parameters defining the interaction between colloidal particles. Numerical results from molecular-dynamics (MD) simulations are compared with analytical models and good agreement is found between both data sets. The results for the timescales are used to calculate the associated rates to generate kinetic Monte Carlo (KMC) simulations, which allow exploring larger systems and longer timescales in comparison with MD simulations. The KMC simulations reproduce the global behavior of the densities of islands and monomers as well as the gap length distribution between adjacent islands.

DOI: 10.1103/PhysRevE.109.064604

I. INTRODUCTION

Epitaxy involves the growth of crystalline layers on a substrate, allowing precise control over the arrangement and properties of the deposited material. This process has contributed significantly to modern technology as it is indispensable in the fabrication of advanced electronic and optoelectronic devices. In standard epitaxial growth, atoms are deposited on a substrate at a controlled rate. After deposition, these adatoms or monomers diffuse on the substrate until they cluster with other monomers forming stable islands or until they aggregate to preexisting ones. These two processes are called nucleation and aggregation, respectively, and these are of great interest since their characteristic parameters ultimately determine the properties of the epitaxially grown structures [1–3].

Despite the conceptual simplicity of the fundamental processes involved in epitaxial growth, the theoretical models proposed so far to describe them are not able to completely predict various magnitudes of interest for controlling the layer growth, for example, the critical size of islands, the time evolution of the density of islands, the size distribution of islands, and the distribution of the so-called capture zones [4–18].

The knowledge of many phenomena in condensed-matter physics has been improved in recent decades due to using colloidal systems as models for mimicking their atomic counterparts [19]. Due to the tunability of both the extent and the intensity of the interactions between colloidal particles, these are convenient systems for studying fundamental phenomena such as crystallization, gelation and vitrification, and formation of crystal defects [20–22]. In particular, sedimentation of particles from a dilute colloidal suspension on a flat or patterned surface is a common method to form colloidal crystals [23–25]. These studies have led to the conclusion that the nature of colloidal epitaxy is, in many aspects, similar to that found in atomic epitaxy. Closely related, the drop-drying method is also of interest for the formation of highly ordered monolayers; as the droplet evaporates, the suspended colloidal particles are swept away and adsorbed at the interface, where they diffuse and aggregate on the gas-liquid surface of the droplet [26,27].

In addition to the possibility of tuning the interactions between colloidal particles, the length and timescales involved in colloidal systems allow the experimental observation of nucleation and growth dynamics of self-assembled colloidal monolayers with a resolution equivalent to the particle size [28–30]. For instance, the mechanisms leading to the creation of Ehrlich-Schwoebel barriers, which determine the interlayer transport of monomers, were found to have a kinetic origin in colloidal systems [28,29]. It was also demonstrated that the surface energy landscape can help precisely control nucleation and consequently the size and symmetry of the growing islands [31]. These studies have also considered heteroepitaxy, where, for example, parallel mechanisms between colloidal and atomic systems were found for strain relief for lattice misfit between the growing film and the substrate [32,33].

On the other hand, simulation-based studies of colloidal systems have given results on the role of different physical parameters, such as the effect of the stress field of the substrate in the dynamics of island formation and the morphology of the resulting islands [34]. Empirical interaction potentials have also been considered to understand the dependence on the colloidal size of the critical island size and the energy barriers for both island relaxation and interlayer diffusion [35]. In practice, the results obtained through simulations of colloidal epitaxy can be experimentally replicated. Considering that these observables are to some degree scalable between the

*juan.david.alvarez@correounivalle.edu.co
†manuel.camargo@uan.edu.co
‡diego.luis.gonzalez@correounivalle.edu.co

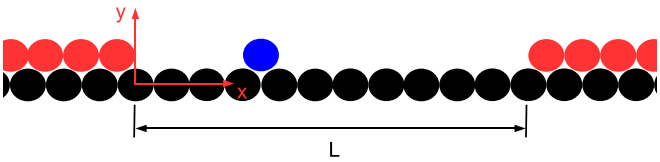

FIG. 1. One free monomer (blue circle) inside a gap of length L between two fixed islands (red circles). Both red and blue are A-type particles, while the substrate is formed by B-type particles (black circles).

molecular and atomic, mostly for submonolayer growth [36], they provide a better understanding of the interactions and processes related to island formation and monolayer growth.

Recently, a two-dimensional colloidal model was introduced to explore the time evolution of both monomer and island densities when a two-step protocol is used for epitaxial growth. Such a protocol has the major advantage that nucleation and aggregation processes take place at different timescales [37]. The main assumption of this model is that the interactions between the colloidal particles are known quantities; therefore, molecular-dynamics (MD) simulations can be employed to follow the deposition of colloids on a one-dimensional substrate due to the slow sedimentation from a two-dimensional dilute suspension. By comparing the simulation results with analytical considerations based on rate equations, it was concluded that the analysis of both monomer and island densities, which are experimentally accessible, can indeed help gain information about the system's microscopic dynamics as well as the validity range of the point-island assumption.

It is important to note that a distinctive feature of a one-dimensional substrate is that islands divide it into independent segments called gaps (see Fig. 1). It turns out that the information gathered for nucleation and aggregation processes occurring inside a single gap can be exploited to recover the time evolution of the whole system in the submonolayer regime [14,17,38–40]. More specifically, the capture kernels associated with nucleation and aggregation in a gap are directly related to the time evolution of the densities of islands and monomers. Furthermore, the knowledge of the nucleation and aggregation rates, in conjunction with the appropriate fragmentation equation, makes it possible to evaluate the gap length distribution between adjacent islands. Experimental and numerical methods can be employed to measure all of these quantities, providing valuable insights to test the validity of the proposed theoretical model.

In this work, molecular dynamics is employed to analyze deposition, nucleation, and aggregation events occurring inside a single gap for a one-dimensional substrate. The simulations allow us to calculate the transition rates associated with deposition, nucleation, aggregation, and diffusion as a function of the interaction parameters between colloidal particles. To explore the evolution of the densities of islands and monomers, the evaluated transition rates are used as input for kinetic Monte Carlo (KMC) simulations. Both MD and KMC results are compared with those from a fragmentation equation based on the description of aggregation and nucleation inside a single gap. In particular, a comparison is made for the gap length distribution between adjacent islands.

This paper is structured as follows. Section II describes the single-gap model employed. In Sec. III the relevant timescales are calculated both numerically and analytically for several interaction parameters. The distribution of nucleation sites is also discussed there. In Sec. IV we provide an analytical expression for the distribution of the nucleation sites for gaps having different lengths. The comparison between the results of KMC simulations and those from MD is presented in Sec. V. In Sec. VI we show how our results for a single gap can be used to describe the gap length distribution. In Sec. VII we draw some conclusions.

II. MODEL DESCRIPTION

Consider a single mobile colloidal particle (monomer) confined inside the gap between two adjacent islands deposited on a substrate, as depicted in Fig. 1. The islands are considered immobile, stable, and formed by monomers of type A, while immobile particles of type B form the substrate. All monomers have diameter σ and mass m and are influenced by an external constant sedimentation field $\vec{F}$. The absolute temperature of the suspension above the substrate is T, and D_0 denotes the diffusion coefficient of a particle in the suspension. In the following σ, m, k_BT, and $\tau_{\rm MD}$ are taken as length, mass, energy, and time units, respectively, with $\tau_{\rm MD} = \sqrt{m\sigma^2/k_BT}$ and k_B the Boltzmann constant.

The particle-particle interaction is modeled by the Morse potential

$$V_{ij}(r) = \begin{cases} \mathcal{A}_{ij}(e^{-2\alpha(r-\sigma)} - 2e^{-\alpha(r-\sigma)}), & r \leqslant r_{\rm cut} \\ 0, & r > r_{\rm cut}, \end{cases} \tag{1}$$

where r is the center-to-center distance between two colloidal particles. The parameters $\mathcal{A}_{ij}$ $(i, j = A, B)$, α, and $r_{\rm cut}$ determine the strength, range, and cutoff distance of the interaction potential, respectively. While the selection of the potential may seem arbitrary, it maintains two primary characteristics: a hard-core interaction and a short-range attractive contribution. These features are exemplified, for instance, by the Asakura-Oosawa potential, which effectively describes the depletion potential resulting from adding small polymers into the colloidal suspension [36,37].

The colloids evolve according to Langevin dynamics in such a way that the position of the ith colloid, $\vec{r}_i$, changes according to

$$m\frac{d^2\vec{r}_i}{dt^2} = -\zeta_0\frac{d\vec{r}_i}{dt} + \nu\vec{\eta}(t) + \vec{F}_i(t), \tag{2}$$

where $\vec{F}_i(t)$ is the total force on the ith colloid due to the external field and all the other colloidal particles [41]. The solvent is taken into account implicitly through the parameters ζ_0 and ν, which give the intensity of the viscous and stochastic forces [first and second terms of Eq. (2)], respectively. As usual, the stochastic variable $\vec{\eta}(t)$ is defined according to

$$\langle\vec{\eta}(t)\rangle_\eta = 0, \quad \langle\vec{\eta}(t)\vec{\eta}(t')\rangle_\eta = \mathbf{I}\delta(t-t'), \tag{3}$$

where $\langle\cdot\rangle_\eta$ indicates the ensemble average, $\delta(t)$ is the Dirac delta function, $\mathbf{I}$ is the 2×2 identity matrix, and the intensity of the random force, ν, is chosen to satisfy the fluctuation-dissipation theorem.

The deposition of colloids inside the gap proceeds as follows. A colloid is introduced in the simulation box at random x, height $y_{\rm ins} = 1.02\sigma$, and with a vertical velocity equal to $-F/m\zeta_0$, which corresponds to the monomer's steady-state velocity in the suspension. Inserting the colloid with these initial conditions helps shorten the simulation time since these implicitly assume that the monomers are deposited at a height high enough to reach the substrate with a velocity equal to that of the steady state. The sedimentation field ensures that the colloid moves toward the substrate and is eventually incorporated into the gap. The substrate generates a periodic potential with well-defined minima, each comprising a metastable site for the deposited mobile monomer. After thermalization, the free monomer moves on the substrate by hopping between consecutive sites, with τ the average hopping time. Therefore, the (lateral) diffusion constant of the monomer on the substrate is given by $D = \sigma^2/2\tau$.

For the numerical description of nucleation, configurations involving only two free monomers within the gap are required, so we proceed as follows. The average time elapsed between the deposition of these two colloids is $\tau_{\rm dep}$. To improve the computational efficiency of the MD simulation, we deposit both colloids simultaneously. However, one of them was deposited at random x having a uniform distribution, while the other one was deposited at random x following the distribution of free colloids of the steady state [see Eq. (20)]. This way, it is implicitly assumed that the first monomer has enough time to reach the steady-state regime before the arrival of the second one.

III. TIMESCALES

A. Diffusion constant

From Eq. (2), the Fokker-Planck equation associated with the distribution $P(x, y, t)$ of finding a particle at position (x, y) at time t is given by [41]

$$\zeta_0 \frac{\partial P(x,y,t)}{\partial t} - \left[\frac{\partial}{\partial x}\left(\frac{\partial \mathcal{V}(x,y)}{\partial x} + \frac{\nu^2}{2\zeta_0}\frac{\partial}{\partial x}\right) + \frac{\partial}{\partial y}\left(\frac{\partial \mathcal{V}(x,y)}{\partial y} + \frac{\nu^2}{2\zeta_0}\frac{\partial}{\partial y}\right)\right] P(x,y,t) = 0. \quad (4)$$

Equation (4) is not separable due to the presence of the term associated with the interaction potential $\mathcal{V}(x, y)$, preventing one from finding an exact solution for $P(x, y, t)$ with the Morse potential. However, for a suitable choice of the system parameters, the free colloids will move on the substrate by infrequent events. Therefore, the distribution probability of finding a monomer close to a potential minimum, i.e., once it has been adsorbed by the substrate, can be approximated by the equilibrium distribution

$$P(x, y, t) \approx C \exp[-\beta \mathcal{V}(x, y)], \quad (5)$$

where C is the normalization constant of the distribution. Figure 2 shows the marginal probabilities

$$p_x(x) = \int_0^{r_{\rm cut}} dy\, P(x, y, t) \quad (6)$$

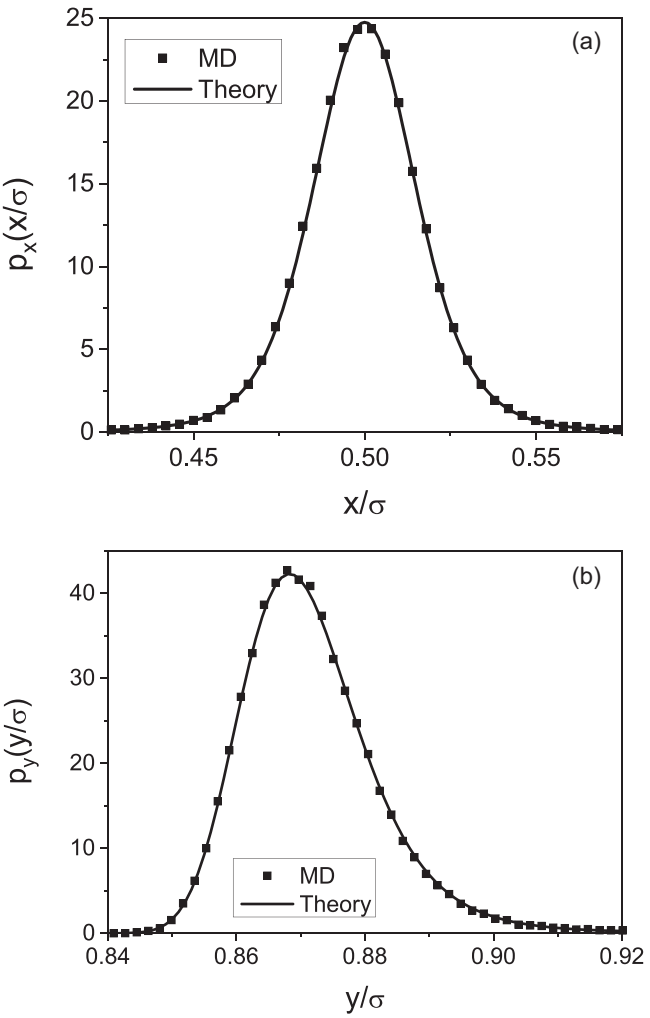

FIG. 2. Marginal distributions (a) $p_x(x)$ and (b) $p_y(y)$ given by Eqs. (6) and (7). As expected, $p_y(y)$ has a well-defined peak at $y \simeq (\sqrt{3}/2)\sigma$, while $p_x(x)$ has its maximum at the midpoint between the center of two consecutive colloids of the substrate.

and

$$p_y(y) = \int_{-\sigma/2}^{\sigma/2} dx\, P(x, y, t), \quad (7)$$

which were evaluated using MD simulations for the parameters $\mathcal{A}_{AA} = 8.8k_BT$, $\mathcal{A}_{AB} = 8.0k_BT$, $\alpha = 25/\sigma$, $\zeta_0 = m/\tau_{\rm MD}$, $F = k_BT/\sigma$, and $r_{\rm cut} = 1.6\sigma$. As shown in Ref. [37], this set of parameters allows the stable growth of islands in the submonolayer regime with a negligible detachment of monomers from the substrate. However, in the case of eventual evaporation, we impose a reflective boundary condition at $y = r_{\rm cut} = 1.6\sigma$, which corresponds to the interaction cutoff distance. In Fig. 2, squares and lines correspond to MD and theoretical results, respectively, the latter being obtained using Eqs. (1) and (5)–(7); as can be seen there, the agreement between numerical and analytical results is excellent.

Using Eq. (4) and the periodicity of the potential energy on the substrate, in Ref. [41] it is demonstrated that, in the high-friction limit, the diffusion coefficient for a horizontal

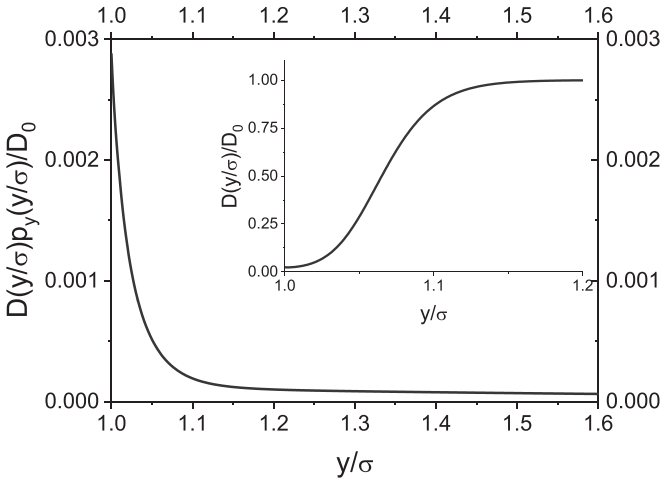

FIG. 3. Behavior of the distribution $D(y)p_y(y)$ as a function of y. The inset shows how $D(y)$ increases with y until it equals the value of the diffusion constant in the suspension. The $D(y)$ is given by Eq. (8) with system parameters taken from Ref. [37].

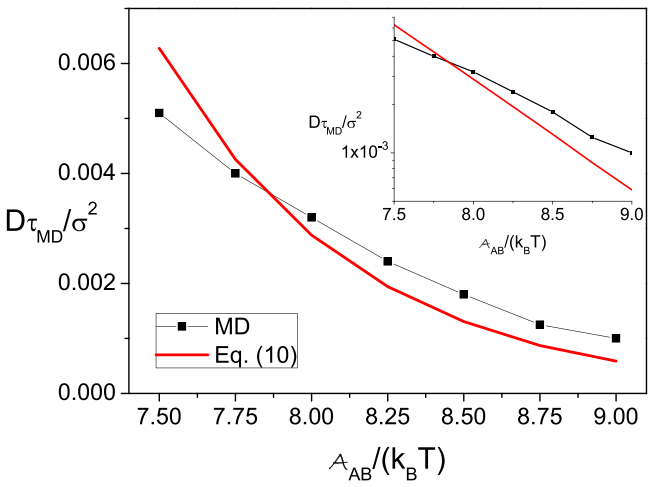

FIG. 4. Diffusion coefficient for different values of the interaction parameter $\mathcal{A}_{AB}$. The results are evaluated from Eq. (10) and molecular-dynamics simulations.

trajectory at a given y can be expressed as

$$D(y) = D_0\sigma^2 I_2^{-1}(y), \tag{8}$$

where D_0 is the diffusion coefficient in the suspension and $I_2(y)$ corresponds to the Lifson-Jackson formula [42]

$$I_2(y) = \int_0^\sigma dx\, \mathrm{e}^{\mathcal{V}(x,y)/k_BT} \int_0^\sigma dx\, \mathrm{e}^{-\mathcal{V}(x,y)/k_BT}. \tag{9}$$

Equation (8) cannot be directly applied to our system because free monomers do not move along a horizontal line due to the fluctuations of the y coordinate. Additionally, the result of the integral in Eq. (9) strongly depends on y, as shown in the inset of Fig. 3. Note that in the region $y > \sigma$, $D(y)$ equals the diffusion constant at the suspension. However, we can estimate the diffusion constant using Eq. (8) as follows. Due to the finite size of the colloids, the transitions between metastable states only occur for $y \gtrsim \sigma$. As shown in Fig. 2 for $p_y(y)$, the probability of finding the particle in this region is quite small. Consequently, the distribution $D(y)p_y(y)$ decays rapidly as y becomes greater than σ, as can be seen in Fig. 3. Then the effective (lateral) diffusion coefficient D can be estimated as

$$D = D(\sigma)p_y(\sigma). \tag{10}$$

Figure 4 displays the results for the diffusion coefficient D obtained by numerically evaluating Eqs. (8) and (10) at $y = \sigma$ for different values of $\mathcal{A}_{AB}$. The theoretical results are compared to those from MD simulations estimated from the long-time behavior of the mean-square displacement. The diffusion constant $D = D(\sigma)p_y(\sigma)$ strongly depends on $\mathcal{A}_{AB}$ as it decreases two orders of magnitude as $\mathcal{A}_{AB}$ increases from $7.0k_BT$ to $9.0k_BT$. The inset shows that our approximation reproduces the exponential decay of D as a function of $\mathcal{A}_{AB}$ but overestimates the decay rate. As mentioned in Ref. [37], taking $A_{AB} = 8.0k_BT$ guarantees the mobility of the free colloids on the substrate but makes unlikely their detachment from the substrate.

B. Deposition rate

The deposition rate due to the slow sedimentation of colloids from the suspension on the substrate can be calculated as follows. Let ρ be the density of colloids in the suspension. For $y > 1.6\sigma$ the colloids do not interact with the substrate, and for small densities ρ, the interaction between mobile colloids can be ignored. Under these conditions, $\mathcal{V}(x, y) \simeq 0$ and in Eq. (4) can be analytically solved. The probability of finding a colloid between y and $y + dy$ in the steady state is given by

$$P(y, t) = \frac{\zeta_0 J}{F}(1 - \mathrm{e}^{-2\zeta_0 F y/\nu^2}), \tag{11}$$

where J is the probability current for a single colloid. The deposition rate $\mathcal{F}$ (number of particles deposited per unit length per time) is given by

$$\mathcal{F} = \frac{2\rho F^2 L_y}{\nu^2(\mathrm{e}^{-2\zeta_0 F L_y/\nu^2} - 1) + 2\zeta_0 F L_y}, \tag{12}$$

with L_y the height of the suspension. For $k_BT \ll FL_y$, Eq. (12) reduces to the simple linear form $\mathcal{F} = \rho F/\zeta_0$. The average time between consecutive depositions in a gap of length L is given by $\tau_{\mathrm{dep}} = (\mathcal{F}L)^{-1}$. Figures 5 and 6 show the behavior of τ_{dep} and $\mathcal{F}$ as a function of F, respectively. In both cases, good agreement is found between MD results and those from the analytical model. As expected, the linear approximation for the deposition rate gives good results for large values of F.

C. Aggregation time

The traversal time τ_{tr} is defined as the average time after deposition required for a monomer to reach one of the gap edges, while the residence time τ_{res} measures the survival time of a monomer before it aggregates to one of the islands of the gap. Both quantities can be estimated using a simple random-walk model for a colloid confined inside a gap. Let $p_n(t)$ be the probability of finding a single monomer at time t in the nth site of the gap, which can be calculated from the master

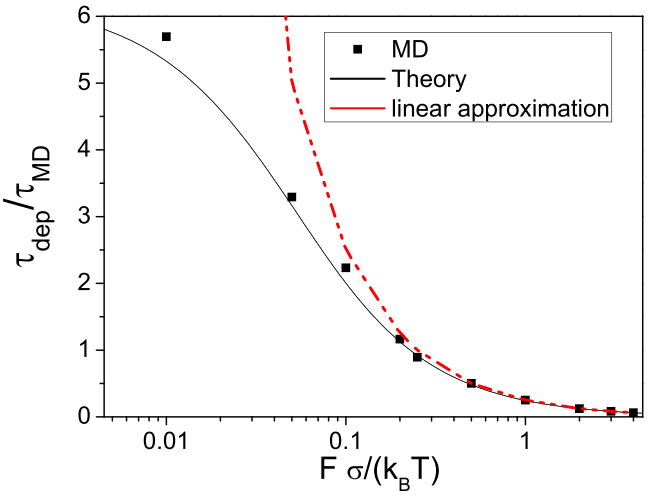

FIG. 5. Deposition time as a function of F evaluated from MD simulations and from the analytical result [Eq. (12)].

equation

$$\frac{dp_n(t)}{dt} = \frac{1}{2\tau}[p_{n+1}(t) + p_{n-1}(t) - 2p_n(t)], \tag{13}$$

where $\tau = \sigma/2D$ is the average hopping time. The boundary conditions are $p_0(t) = \epsilon p_1(t)$ and $p_{N+1}(t) = \epsilon p_N(t)$, where N is the number of lattice sites (potential minima in the gap) and $L = N\sigma$. The parameter $0 \leqslant \epsilon \leqslant 1$ characterizes the interaction between the islands and free colloids. For $\epsilon = 0$ the islands behave as perfect traps, i.e., once a monomer reaches the interaction range of an island, it is instantly captured by the island. Then $\tau_{res} = \tau_{tr}$ since aggregation takes place instantaneously. On the other hand, for $\epsilon = 1$ we have perfect reflecting boundary conditions and aggregation is impossible in this case.

From $p_n(t)$, the survival probability $P_s(t)$, defined as the probability of finding the monomer inside the gap at time t, can be evaluated as

$$P_s(t) = \sum_{n=1}^{N} p_n(t). \tag{14}$$

Then the probability for a monomer to be captured in the time interval $[t, t + \Delta t]$ determines the residence probability distribution $P_{res}(t)$ as

$$P_{res}(t)\Delta t = -P_s(t + \Delta t) + P_s(t), \tag{15}$$

which in the limit $\Delta t \to 0$ takes the form

$$P_{res}(t) = -\frac{dP_s(t)}{dt}. \tag{16}$$

The residence time τ_{res} is the average time a monomer spends inside the gap before being captured by an island. Therefore, using Eq. (16), τ_{res} can be calculated from

$$\begin{aligned}\tau_{res} &= \int_0^\infty dt\, t P_{res}(t) \\ &= \int_0^\infty dt\, P_s(t) \\ &= \sum_{n=1}^{N} \rho_n,\end{aligned} \tag{17}$$

where the density at site n, ρ_n, is defined as

$$\rho_n = \int_0^\infty dt\, p_n(t), \tag{18}$$

where the integration domain was extended up to infinity as $p_n(t)$ is a rapidly decreasing function of t for the parameters used.

Using the definition given by Eq. (18) in Eq. (13), it is found that ρ_n satisfies the recurrence relation

$$-2\tau p_n(0) = \rho_{n+1} + \rho_{n-1} - 2\rho_n, \tag{19}$$

with boundary conditions $\rho_0 = \epsilon\rho_1$ and $\rho_{N+1} = \epsilon\rho_N$. The linear nonhomogeneous recurrence relation given by Eq. (19) can be solved using standard procedures [43]. The solution can be written as $\rho_n = \sum_{j=0}^{2} c_j n^j$, where the coefficients c_j are calculated by replacing the proposed solution in Eq. (19) and using the boundary conditions mentioned above. The explicit form of ρ_n is given by

$$\rho_n = \frac{\tau}{N}\left(\frac{\epsilon N}{1-\epsilon} + (N+1)n - n^2\right). \tag{20}$$

From Eqs. (17) and (20), the residence time is

$$\tau_{res} = \tau\left(\frac{\epsilon N}{1-\epsilon} + \frac{(N+1)(N+2)}{6}\right). \tag{21}$$

Figure 7 shows the behavior of the parameter ϵ for different values of $\mathcal{A}_{AB}$, which was calculated using Eq. (20) and the MD results for ρ_n. Large values of $\mathcal{A}_{AB}$ ensure that islands behave like perfect traps, i.e., $\mathcal{A}_{AB} \to \infty$ and $\epsilon \to 0$. For small values of the interaction parameter, the detachment of colloids from the islands is very likely and the density of free colloids inside the gap turns out to be homogeneous, as shown in the inset of Fig. 7. For the three values of $\mathcal{A}_{AB}$ considered, Eq. (20) gives an excellent description of the normalized density.

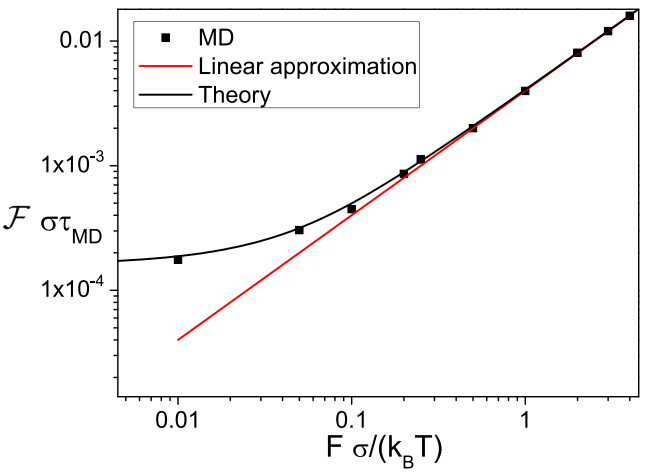

FIG. 6. Deposition rate as a function of F. As predicted, the deposition rate increases linearly for large values of F.

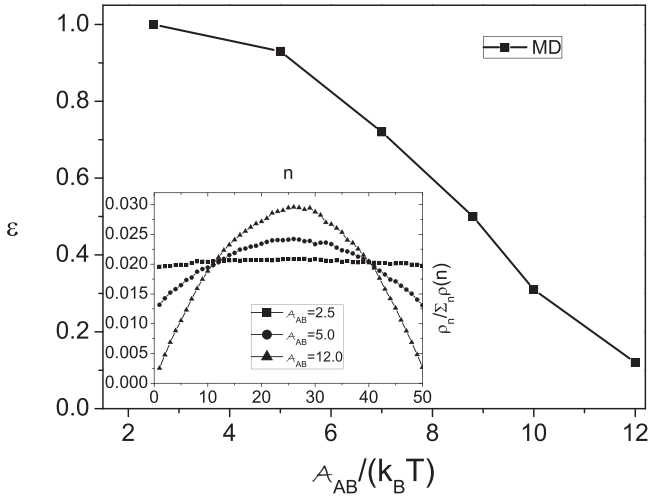

FIG. 7. Molecular-dynamics results for the parameter ϵ as a function of the interaction strength $\mathcal{A}_{AB}$. The inset shows the normalized density $\rho_n/\sum_n \rho_n$ for three different values of $\mathcal{A}_{AB}$. Symbols correspond to MD results and lines to Eq. (20).

However, for large values of $\mathcal{A}_{AB}$ the diffusion coefficient D becomes comparable to the deposition rate $\mathcal{F}$. This is not a desired situation since it leads to an evolution in which nucleation and aggregation occur simultaneously, decreasing the chance of controlling the formed structure. To avoid this issue, from now on we take $\mathcal{A}_{AB} = 8.0k_BT$ and set the density in the suspension in such a way that $\mathcal{F} \simeq 2 \times 10^{-6}$, which gives $\mathcal{R} = D/\mathcal{F} \approx 1.6 \times 10^3$. Despite ϵ being finite for this interaction strength, taking $\epsilon = 0$ in Eqs. (20) and (21) gives an excellent approximation for evaluating both ρ_n and $\tau_{\rm res}$. Figure 8 shows the density for gaps with different lengths ($N = 10$, 20, 30, 40, and 50). The numerical evidence suggests that the islands can be considered perfect traps for the employed parameters and then the system is limited by diffusion. Similarly, the behavior of $\tau_{\rm res}$ as a function of N with $\epsilon = 0$ is shown in Fig. 9. The agreement with Eq. (21) is excellent, especially for large gaps where $\tau_{\rm res} \approx \tau N^2/6$.

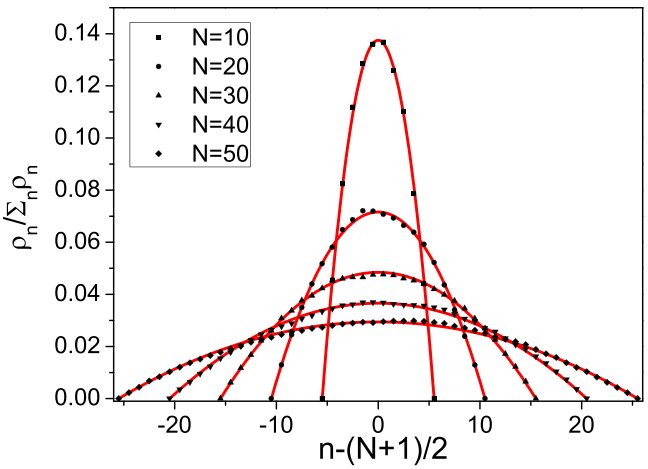

FIG. 8. Density ρ_n for five different gap lengths. Symbols correspond to MD results and lines to analytical results from Eq. (20) with $\epsilon = 0$.

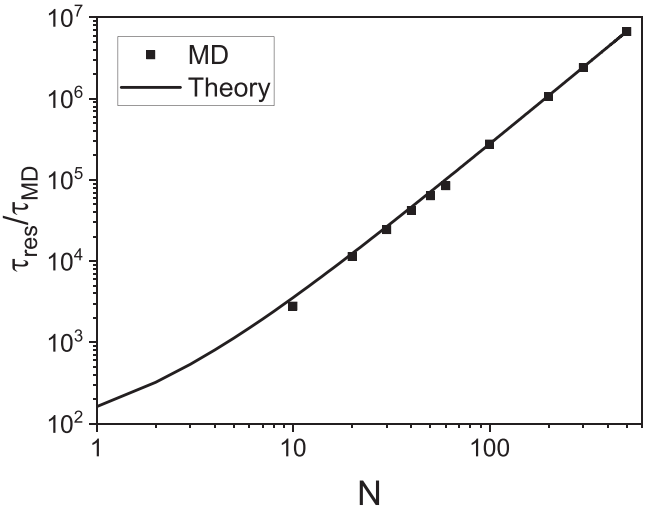

FIG. 9. Behavior of $\tau_{\rm res}$ as a function of N. Symbols correspond to MD results and the line to Eq. (21). The inaccuracy induced by taking $\epsilon = 0$ becomes negligible for large gaps ($N > 20$).

IV. SPATIAL DESCRIPTION OF NUCLEATION

For small densities of colloidal particles in the suspension, the deposition rate of monomers satisfies $\mathcal{F} \ll D$. Therefore, $\tau_{\rm res} \ll \tau_{\rm dep} = \mathcal{F}L$ for a gap of length L and the probability of simultaneously finding more than one colloid inside a gap is small. In this limit, the probability of finding i monomers in the gap at the moment of the $(i+1)$th deposition, q_{i+1}, is given by [44]

$$q_{i+1} = \frac{1}{i!}\left(\frac{\tau_{\rm res}}{\tau_{\rm dep}}\right)^i = \frac{1}{i!}\left[\frac{L^2}{12\mathcal{R}}\left(L + \frac{6\epsilon\sigma}{1-\epsilon}\right)\right]^i. \tag{22}$$

As expected, q_{i+1} strongly depends on ϵ, L, and $\mathcal{R}$. For the parameters used in the simulations $\tau_{\rm dep} \gg \tau_{\rm res} \approx \tau_{\rm tr}$ and $q_{i+1} \approx (L^3/12\mathcal{R})^i/i!$. In epitaxial growth, the critical size is the maximum size of an unstable island. In our MD simulations we set $\mathcal{A}_{AA} = 8.8k_BT$, which makes dimers stable, i.e., clusters of two monomers can be considered as immobile and stable islands.

On the other hand, given that $\tau_{\rm res} \ll \tau_{\rm dep}$, if two monomers coincide in the gap, whenever the second monomer arrives, it is very likely that the first one has already reached the steady state. This situation is equivalent to having a gap where both monomers are deposited simultaneously at random sites; the first one is deposited at site n with uniform probability $1/N$ and the second with a probability given by $\rho_n/\sum_n \rho_n$. The time evolution of two free colloids is given by the master equation

$$\frac{dp_{m,n}(t)}{dt} = \frac{1}{4\tau}[p_{m+1,n}(t) + p_{m-1,n}(t) + p_{m,n+1}(t) + p_{m,n-1}(t) - 4p_{m,n}], \tag{23}$$

where $p_{0,n}(t) = p_{N+1,n}(t) = p_{m,0}(t) = p_{m,N+1}(t) = 0$ and $p_{n,n} = 0$. In the following, we assume that nucleation occurs once the colloids are separated by a distance smaller than the interaction range, which is a reasonable assumption as the set $\mathcal{A}_{AB}$ makes detachment negligible. The solution of Eq. (23)

can be found using the auxiliary initial condition [45–47]

$$\tilde{p}_{m,n}(0) = \begin{cases} -p_{n,m}(0) & \text{for } m > n \\ 0 & \text{for } m = n \\ p_{m,n}(0) & \text{for } m < n, \end{cases} \tag{24}$$

where the symmetrized $p_{m,n}(0)$ can be written as

$$p_{m,n}(0) = \frac{\rho_n + \rho_m}{2L\sum_n \rho_n}. \tag{25}$$

In this way, the probability of having two colloids in sites m and n in the gap has the form

$$p_{m,n}(t) = \sum_{k,j=1}^{N} B_{k,j} e^{c_{kj}t/4\tau} X_{m,n}, \tag{26}$$

where

$$X_{m,n} = \sin\left(\frac{\pi km}{N+1}\right)\sin\left(\frac{\pi jn}{N+1}\right). \tag{27}$$

The constants c_{kj} and B_{kj} are given by

$$c_{kj} = 2\left[\cos\left(\frac{\pi k}{N+1}\right) + \cos\left(\frac{\pi j}{N+1}\right) - 2\right] \tag{28}$$

and

$$B_{kj} = \left(\frac{2}{N+1}\right)^2 \sum_{m<n} \tilde{p}_{m,n}(0) X_{m,n}, \tag{29}$$

respectively. The probability that nucleation occurs at site n, $\mathcal{P}(n)$, is given by

$$\mathcal{P}(n) = \frac{1}{4\tau}\int_0^\infty dt[p_{n+1,n}(t) + p_{n-1,n}(t) + p_{n,n+1}(t) + p_{n,n-1}(t)]. \tag{30}$$

Using Eqs. (26)–(30), the probability of nucleation can be written as

$$\mathcal{P}(n) = \frac{1}{2}\sum_{k,j=1}^{N} \frac{B_{kj}(X_{n,n+1} + X_{n,n-1})}{1 - \frac{1}{2}\left[\cos\left(\frac{k\pi}{N+1}\right) + \cos\left(\frac{j\pi}{N+1}\right)\right]}. \tag{31}$$

Note that we do not consider the direct deposition of one colloid on top of another at $t = 0$. Numerical evidence from KMC simulations has shown that an excellent mean-field approximation for Eq. (31) is given by the Walton relation, i.e., it is assumed that $\mathcal{P}(n)$ is proportional to the squared density [14,38,48]

$$\mathcal{P}_{\rm MF}(n) \approx \frac{30n^2(N-n+1)^2}{(N+1)^5}. \tag{32}$$

This distribution can be scaled using the transformation $\lambda = n/N$ and $p(\lambda) = N\mathcal{P}(\lambda)$ so that Eq. (32) can be rewritten as

$$p_{\rm MF}(\lambda) \approx 30\lambda^2(1-\lambda)^2. \tag{33}$$

Figure 10 shows the scaled distribution of the nucleation sites for gaps having different lengths ($N = 20$, 40, and 60). Both $\mathcal{P}(n)$ and $\mathcal{P}_{MF}(n)$ provide an adequate description of the simulation results. These results also support the approximation $\epsilon = 0$, since $\mathcal{P}(n)$ should be flatter and $\mathcal{P}(0) > 0$ otherwise. The main differences between the analytical and numerical results are due to the assumption that a nucleation occurs when a colloid hops on top of the other used in the former, while in the simulations a nucleation occurs when the centers of two colloids are closer than the interaction cutoff distance, which leads to a more pronounced distribution peak. The initial condition given by Eq. (24) is formally fulfilled in the limit $\mathcal{R} \to \infty$, which cannot be easily achieved for colloids; as mentioned previously, in this work $\mathcal{R} \approx 1.6 \times 10^3$ is far from the desired limit.

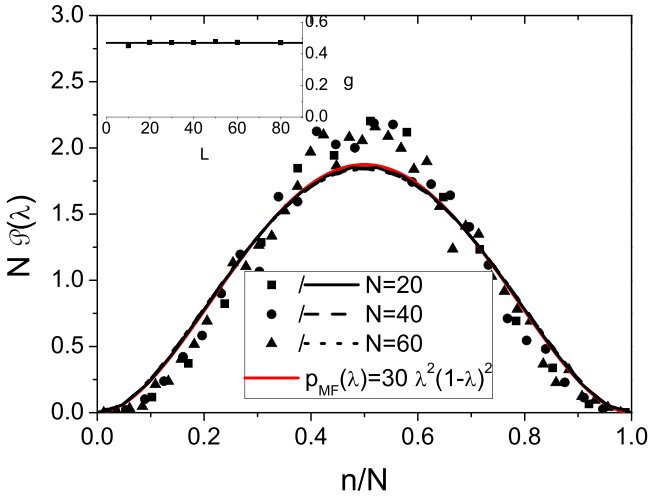

FIG. 10. Probability distribution for nucleation taking place at site n. Symbols correspond to MD simulation results, black lines to theoretical results from Eq. (31), and the red line to the mean-field approximation given by Eq. (33). The inset shows that the nucleation rate inside the gap ($g \simeq 0.47$) is found to be independent of the gap length.

The nucleation rate inside the gap, ω, indicates the number of nucleation events per time unit. Let g be the conditional probability for a nucleation inside a gap given that two monomers are inside the gap at the time of the second deposition. Consequently, ω can be written as

$$\omega = gq_2\mathcal{F}L, \tag{34}$$

where q_2 is given by Eq. (22) and g can be evaluated from $\mathcal{P}(n)$ according to

$$g = \sum_{n=1}^{N} \mathcal{P}(n). \tag{35}$$

The numerical evaluation of Eq. (35) using the result of Eq. (31) leads to $g \approx 0.47$ regardless of the gap length, as shown in the inset of Fig. 10. This is a consequence of the chosen interaction parameters, which make dimers stable. For a different set of interaction parameters, the critical nucleus size can be larger than $i = 1$ and g would depend on L [17].

V. KMC SIMULATION FROM MD RESULTS

Two typical quantities used in epitaxial growth to describe the time evolution of the growing monolayer are the monomer ($\mathcal{N}_1$) and island ($\mathcal{N}$) densities. Starting from the results described in the preceding section, we implement kinetic Monte Carlo simulations for monolayer growth using the same interaction parameters and the ratio $\mathcal{R} = D/\mathcal{F} \simeq 1.6 \times 10^3$. In

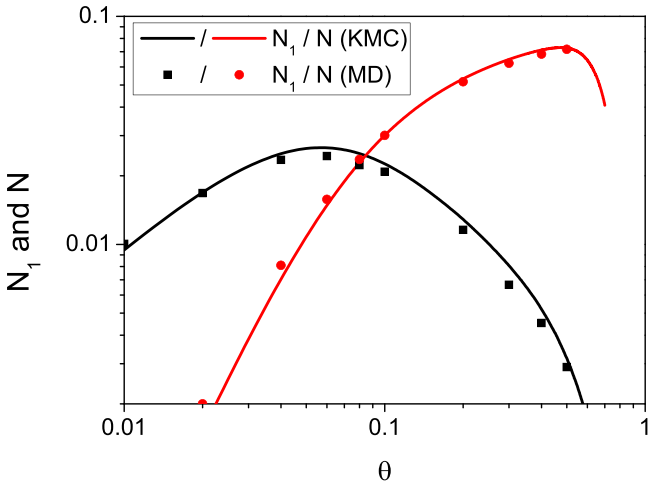

FIG. 11. Evolution of monomer $\mathcal{N}_1$ and island $\mathcal{N}$ densities as a function of the coverage $\theta = \mathcal{F}t$. Symbols correspond to MD simulations and lines to the KMC results.

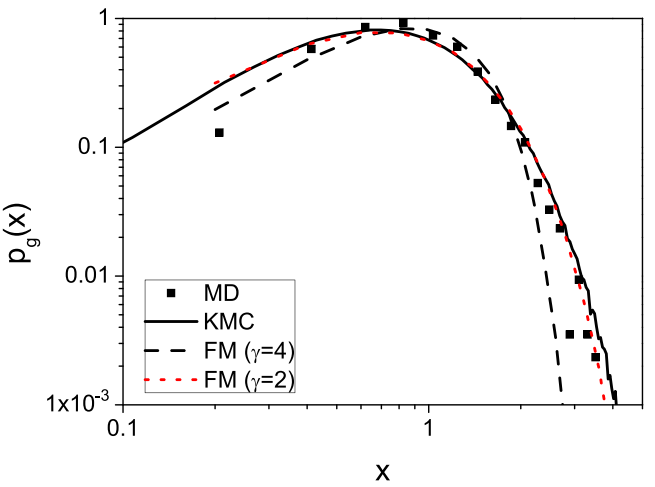

FIG. 12. Gap length distribution for adjacent islands for a coverage $\theta = 0.25$. Symbols and the solid line correspond to MD and KMC results, respectively. Dashed and dotted lines are obtained from the solution of the fragmentation model given by Eq. (36) with different values of γ.

these simulations, we consider a one-dimensional lattice (substrate) with $N = 1000$ sites on which colloids are deposited at random. On average, $2\mathcal{R}\mathcal{N}_1$ random moves are made by the free colloids on the lattice between two consecutive depositions. In this way, the hopping time is guaranteed to be $\tau = \sigma^2/2D$ and the time between consecutive depositions is $(\mathcal{F}L)^{-1}$. Note that the interaction parameters determine not only the diffusion coefficient of the colloids on the substrate but also the critical nucleus size i. For the set of parameters used in the MD simulations, once two colloids are in consecutive lattice sites they form a stable island. Therefore, we implement the extended island model in the KMC simulations, i.e., if a free colloid moves onto a site that is adjacent to one already occupied by another colloid, then either an aggregation or a nucleation event is considered to occur.

VI. FROM LOCAL TO GLOBAL BEHAVIOR

Evolution of densities

Figure 11 shows the evolution of $\mathcal{N}$ and $\mathcal{N}_1$ as a function of the coverage $\theta = \mathcal{F}t$, where t is the physical time and θ is the total density of deposited particles. As can be seen there, the agreement between the two simulation methods is excellent. A major advantage of the KMC over the MD simulations is that the KMC simulation allows one to simulate much larger systems and longer timescales with less computational effort.

Another quantity that is also useful for studying epitaxial growth is the gap length distribution for gaps of length l between neighboring islands. This distribution provides information about the effective interaction between islands as well as about the capture zone distribution [14,38,39]. The gap length distribution can be recovered using a fragmentation model which uses as input the results of Sec. III. Following Ref. [38], we define the scaled gap length distribution $p_g(x)$, which satisfy the fragmentation equation

$$x\frac{dp_g(x)}{dx} + 2p_g(x) = -Q^g(x) + 2Q^x(x), \tag{36}$$

with $Q^g(x)$ the probability density of nucleation inside a gap with scaled length $x = L/\langle L\rangle$ and $Q^x(x)$ the probability that, given a gap with length y, nucleation occurs at a position x inside the gap [39], i.e.,

$$Q^x(x) = \int_x^\infty dy \frac{1}{y} p_g(y)\mathcal{P}(x/y). \tag{37}$$

In particular, $Q^g(x)$ can be written as

$$Q^g(x) \propto \omega p_g(x), \tag{38}$$

where ω is the nucleation rate inside a gap with scaled length x. Evaluating Eq. (34) for the parameters considered, it is found that $\omega \simeq 0.04\mathcal{F}^2L^4/D$ and consequently

$$Q^g(x) = \frac{x^4}{\mu_4} p_g(x), \tag{39}$$

with μ_4 the fourth moment of $p_g(x)$.

The resulting integro-differential equation for $p_g(x)$ given by Eqs. (36), (37), and (39) cannot be analytically solved. However, it can be solved numerically as shown in Ref. [39]. For large values of x, $p_g(x) \propto x^{-2}\exp(-x^\gamma/\gamma\mu_\gamma)$, with γ the exponent of L in the nucleation rate ω and therefore its behavior is completely determined by $Q^g(x)$. Furthermore, in the limit $x \ll 1$ we have $p(\lambda) \sim \lambda^2$, which in turn implies $p_g(x) \sim x^2$ and $Q^x(x) \sim x^2$. Figure 12 displays the behavior of $p_g(x)$ evaluated for coverage $\theta = 0.25$. As expected, the KMC results coincide with those from MD simulations, especially for large values of x. However, the fragmentation model [Eqs. (36) and (39)] fails to describe the simulation results for $p_g(x)$ at large x. This discrepancy can be understood considering that Eq. (36) implicitly assumes that the system has reached a quasisteady state, in which nucleation and aggregation balance each other; this assumption is reasonable for $\mathcal{R} \to \infty$. In this limit $p_g(x)$ reaches a scaling regime, but for the set of parameters used in our simulations, $\mathcal{R}$ is not large enough to meet this requirement. Additionally, the fragmentation approach assumes that the colloidal density of

the gaps reaches the long-time behavior, which is true for small gaps but not necessarily for large gaps if $\mathcal{R}$ is not large enough. The statistical behavior of the system for large values of x is dominated by the breakup of the largest gaps, and under the steady-state assumption, Eq. (39) predicts $\gamma = 4$. However, for small values of $\mathcal{R}$, we can expect a smaller γ. The numerical evidence suggests that this issue can be overcome by proposing

$$Q^g(x) \propto x^\gamma p_g(x), \tag{40}$$

with $\gamma = 2$. For this empirical value, the fragmentation approach gives excellent results for describing $p_g(x)$ when compared to simulations, as can be seen in Fig. 12.

VII. CONCLUSION

Utilizing established analytical and numerical tools for investigating the colloid dynamics within a single gap, relevant timescales related to nucleation and aggregation can be accurately estimated from the interaction parameters between particles. This allows one to gain valuable insights into the time evolution of monomer and island densities by examining the local behavior of monomers within a gap, which in turn contributes to understanding the global behavior of the epitaxial monolayer growth. Furthermore, the results for the timescales can be used as input for a fragmentation model [Eq. (36)] to calculate the gap length distribution $p_g(x)$ and consequently the capture zone distribution and the effective interaction between islands [14,39]. For $p_g(x)$, our results suggest an exponent $\gamma = 2$, i.e., $p_g(x) \sim x^{-2}\exp(-x^2)$, which differs from the analytical result of $\gamma = 4$. This is not an unexpected result because the exponent γ determines the right tail of the gap length distribution; in other words, it determines the behavior for large gaps. However, for small values of $\mathcal{R}$ the steady-state assumption used for the nucleation description does not apply to large gaps. Additionally, the simultaneous presence of more than two monomers inside a gap is not negligible for large gaps, which is one of the assumptions used to formulate Eq. (22). In our case, the deposition rate is not small enough ($\mathcal{R} \approx 1.6 \times 10^3$) and therefore nucleation in large gaps can occur before the monomer density reaches the steady-state regime. In principle, $\mathcal{R}$ can be arbitrarily large, implying a very long time between depositions and therefore deposition times that in practice cannot be achieved by MD simulations due the long associated simulation times. Consequently, for colloidal epitaxial growth, the typical values of $\mathcal{R}$ are much smaller than those found for molecular beam epitaxy. It is possible to extrapolate the procedure discussed in this paper to higher dimensions. However, for $d > 1$ space is not divided into gaps, and it is necessary to consider the concept of a capture zone (CZ) and the fragmentation equation is written to describe the effect of a single nucleation in the CZ distribution. Finally, we highlight that linking the interaction parameters between colloids with the relevant timescales of the system allows more control of the size and form of the structure formed, which is one of the main goals in epitaxial growth.

ACKNOWLEDGMENTS

D.L.G.-C. is grateful for support from Vicerrectoría de Investigaciones, Universidad del Valle (Colombia) C.I. 71369. M.C. thanks Universidad Antonio Nariño (VCTI-UAN) for financial support through Project No. 2023202.

[1] J. W. Evans, P. A. Thiel, and M. C. Bartelt, Surf. Sci. Rep. **61**, 1 (2006).
[2] H. Ibach, *Physics of Surfaces and Interfaces* (Springer, Berlin, 2006), Vol. 12.
[3] T. Michely and J. Krug, *Islands, Mounds and Atoms* (Springer Science + Business Media, New York, 2012), Vol. 42.
[4] J. W. Evans and M. C. Bartelt, Phys. Rev. B **63**, 235408 (2001).
[5] J. G. Amar, M. N. Popescu, and F. Family, Surf. Sci. **491**, 239 (2001).
[6] M. N. Popescu, J. G. Amar, and F. Family, Phys. Rev. B **64**, 205404 (2001).
[7] J. G. Amar and M. N. Popescu, Phys. Rev. B **69**, 033401 (2004).
[8] A. Pimpinelli and T. L. Einstein, Phys. Rev. Lett. **99**, 226102 (2007).
[9] V. I. Tokar and H. Dreyssé, Phys. Rev. B **80**, 161403(R) (2009).
[10] M. Li, Y. Han, and J. W. Evans, Phys. Rev. Lett. **104**, 149601 (2010).
[11] A. Pimpinelli and T. L. Einstein, Phys. Rev. Lett. **104**, 149602 (2010).
[12] M. Grinfeld, W. Lamb, K. P. O'Neill, and P. A. Mulheran, J. Phys. A: Math. Theor. **45**, 015002 (2012).
[13] T. J. Oliveira and F. D. A. A. Reis, Phys. Rev. B **83**, 201405(R) (2011).
[14] D. L. González, A. Pimpinelli, and T. L. Einstein, Phys. Rev. E **84**, 011601 (2011).
[15] K. P. O'Neill, M. Grinfeld, W. Lamb, and P. A. Mulheran, Phys. Rev. E **85**, 021601 (2012).
[16] P. A. Mulheran, K. P. O'Neill, M. Grinfeld, and W. Lamb, Phys. Rev. E **86**, 051606 (2012).
[17] D. L. González, A. Pimpinelli, and T. L. Einstein, Phys. Rev. E **96**, 012804 (2017).
[18] J. A. Sánchez, D. L. González, and T. L. Einstein, Phys. Rev. E **100**, 052805 (2019).
[19] W. C. Poon, J. Phys. A: Math. Theor. **49**, 401001 (2016).
[20] V. N. Manoharan, Science **349**, 1253751 (2015).
[21] C. P. Royall, S. R. Williams, and H. Tanaka, J. Chem. Phys. **148**, 044501 (2018).
[22] A. Jangizehi, F. Schmid, P. Besenius, K. Kremer, and S. Seiffert, Soft Matter **16**, 10809 (2020).
[23] A. Van Blaaderen, R. Ruel, and P. Wiltzius, Nature (London) **385**, 321 (1997).

[24] A. Van Blaaderen, J. P. Hoogenboom, D. L. Vossen, A. Yethiraj, A. van der Horst, K. Visscher, and M. Dogterom, Faraday Discuss. **123**, 107 (2003).
[25] N. Nakamura, Y. Sakamoto, and H. Ogi, Sci. Rep. **11**, 8929 (2021).
[26] C. P. Joshi, Y. Shim, T. P. Bigioni, and J. G. Amar, Phys. Rev. E **90**, 032406 (2014).
[27] S. P. Thampi and M. G. Basavaraj, Ann. Rev. Chem. Biomol. Eng. **14**, 53 (2023).
[28] R. Ganapathy, M. R. Buckley, S. J. Gerbode, and I. Cohen, Science **327**, 445 (2010).
[29] M. Einax, W. Dieterich, and P. Maass, Rev. Mod. Phys. **85**, 921 (2013).
[30] S. M. Rupich, F. C. Castro, W. T. Irvine, and D. V. Talapin, Nat. Commun. **5**, 5045 (2014).
[31] C. K. Mishra, A. Sood, and R. Ganapathy, Proc. Natl. Acad. Sci. USA **113**, 12094 (2016).
[32] J. Nozawa, S. Uda, A. Toyotama, J. Yamanaka, H. Niinomi, and J. Okada, J. Colloid Interface Sci. **608**, 873 (2022).
[33] M. Mondal and R. Ganapathy, Phys. Rev. Lett. **129**, 088003 (2022).
[34] D. Deb and H. H. von Gruenberg, J. Phys.: Condens. Matter **21**, 245102 (2009).
[35] B. C. Hubartt and J. G. Amar, J. Chem. Phys. **142**, 024709 (2015).
[36] N. Kleppmann, F. Schreiber, and S. H. L. Klapp, Phys. Rev. E **95**, 020801(R) (2017).
[37] M. Camargo and D. L. González, J. Phys.: Condens. Matter **34**, 144006 (2022).
[38] J. A. Blackman and P. A. Mulheran, Phys. Rev. B **54**, 11681 (1996).
[39] D. L. González and T. L. Einstein, Phys. Rev. E **84**, 051135 (2011).
[40] H. Krcelic, M. Grinfeld, and P. A. Mulheran, Phys. Rev. E **98**, 052801 (2018).
[41] H. Risken and T. Frank, *The Fokker-Planck Equation* (Springer, Berlin, 1996).
[42] S. Lifson and J. L. Jackson, J. Chem. Phys. **36**, 2410 (1962).
[43] S. B. Maurer and A. Ralston, *Discrete Algorithmic Mathematics* (CRC, Boca Raton, 2005).
[44] J. Krug, P. Politi, and T. Michely, Phys. Rev. B **61**, 14037 (2000).
[45] P. Politi and J. Villain, Phys. Rev. B **54**, 5114 (1996).
[46] C. Castellano and P. Politi, Phys. Rev. Lett. **87**, 056102 (2001).
[47] P. Politi and C. Castellano, Phys. Rev. E **66**, 031605 (2002).
[48] D. Walton, J. Chem. Phys. **37**, 2182 (1962).